Innovative Infrastructure Solutions (2024) 9:355
https://doi.org/10.1007/s41062-024-01667-3

TECHNICAL PAPER

Analyzing elastoplastic behavior and residual strength ratios in steel tubular braces under compression: a numerical investigation

Hamed Saffari[1] · **Ramin Davoodi**[1] · **Atefeh Soleymani**[1]

Received: 10 October 2023 / Accepted: 5 August 2024 / Published online: 21 August 2024

Abstract

The criteria for acceptance of different section types based on their section and overall slenderness have not been clearly defined by the standards. Hence, the current study delves into the elastoplastic behavior exhibited by bracing constructed from steel tubular sections. The key considerations in the practical design and ductility assessment of steel brace sections involve slenderness and the width-to-thickness ratio. Various circular and square hollow sections' braces, characterized by different slenderness and width-to-thickness ratios, are simulated using ABAQUS finite element software. Initially, the models' accuracy is confirmed through a comparison of analytical results with available experimental data. Subsequently, the investigation focuses on the impact of specific structural and material properties on the residual strength ratio of brace members. Ultimately, a set of logical relationships is proposed for predicting the residual strength ratio and target displacement of these hollow sections. Observations indicate that, in the case of stocky members, the presence of local buckling exerts a notable impact on both ductility and ultimate collapse. Conversely, in the case of slender members, the influence of local buckling on the post-buckling strength is minimal. A decrease in the slenderness parameter results in a heightened residual strength ratio. As the slenderness parameter increases, the residual strength ratio diminishes; subsequently, an elevation in member slenderness leads to an augmentation in the residual strength ratio.

✉ Hamed Saffari
hsaffari@uk.ac.ir

Ramin Davoodi
r.davoodi01@gmail.com

Atefeh Soleymani
Atefeh_soleymani@eng.uk.ac.ir

[1] Department of Civil Engineering, Shahid Bahonar University of Kerman, Kerman, Iran

Graphical abstract

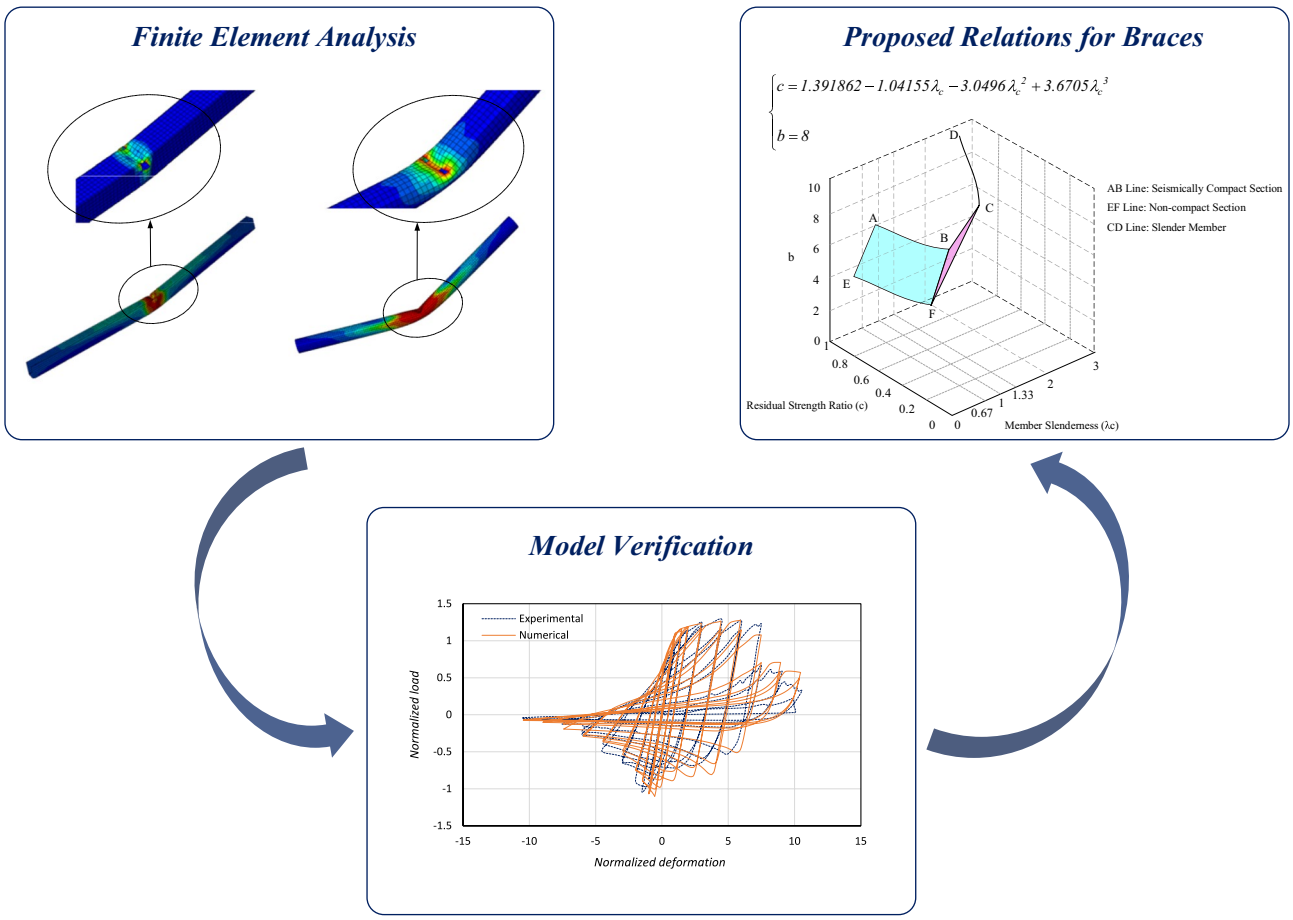

Keywords Steel tubular braces · Elastoplastic behavior · Post-buckling analysis · Finite element modeling · Residual strength ratio · Ductility assessment

Introduction

The brace members of a Concentrically Braced Frame (CBF) system are exposed to axial compression and tension forces. The bracing components must be developed appropriately for the earthquake-resistant building system to perform well. When a brace element attains its critical load in compression loads, the structural member effectively fails and cannot withstand the load [1, 2]. Nonetheless, if there is adequate residual strength, the member can stand the load after buckling [3–5]. The stability of local or global buckling often determines the strength of steel compressive brace members or pipelines [6, 7]. Local buckling is one sort of failure in a member [8]. It depends on factors like the section's width-to-thickness ratio, Poisson's ratio (υ), and Young's modulus (E). Local buckling refers to a phenomenon of plate failure. Many characteristics determine a steel brace's buckling behavior, including yield strength, slenderness ratio, residual stress, and initial out-of-straightness [9, 10]. It has been demonstrated that the width-to-thickness ratio is a critical factor in fracture caused by local instability, including low cycle fatigue and local buckling [11, 12].

Despite this development, it is still unclear whether and how the slenderness ratio influences braces' ability to withstand fatigue over time, which is directly tied to local instability [13]. Tang and Goel [11] noted that fewer multiple local buckling occurred with a higher slenderness ratio and hypothesized that overall buckling had an impact on the brace members' capacity to withstand fracture. They also suggested that whenever the slenderness ratio is less than 60, its impact on the fatigue life should not be taken into account. Several brace experiments employing relatively small-scale cold-formed sections that spanned a wide range of effective slenderness ratios were examined by Jain and Goel [14]. A more accurate fatigue life capacity calculation was put out by Lee and Goel [15], who claimed that compactness is the only factor affecting ductility.

For braces with different slenderness and compactness ratios, Tremblay [16] investigated experimental data. The greatest range in a cyclic deformation history is a function of the with-thickness ratio, according to Fell's [17] assessment of a nearly identical collection of experimental data for braces. His statistical data comparison shows that samples with less ductility had lower slenderness ratios and higher width-thickness ratios. When examining the distribution of these two factors, it is challenging to tell whether the ductility comes from higher width-thickness ratios or slenderness ratios. The dispersion of ductility could also be ascribed to the possibility of steel fabrication, variation of ductility measure, and variability in deformation histories. Chen and Mahin [18] look at how factors employed in designing and analyzing CBFs affect local and global engineering needs. Larger-sectioned brace elements are often stockier and utilized with a lower slenderness ratio. The ductility capacity of braces with a smaller slenderness ratio is often lower, despite offering greater initial compression strength [19–21]. Song et al. [22] worked on the influence of crucial parameters of width-to-thickness ratio (*D/t*) of steel plates in column limb and concrete's prism compressive strength (f_{ck}) on bearing capacity, ductility, and failure mode of the columns in another experimental and numerical study on integrated multi-cell concrete-filled steel tubular (CFST) stub columns under concentric compression. They confirmed the relevance of concrete's constraint impact on CFST members. They also claimed that the rising of the *D/t* of plates can result in a drop in the ductility of CFSTs. Increasing f_{ck}, also decreased the ductility and increased the bearing capacity of CFSTs. Members' test results were also validated by FE analysis. Susanti evaluated the ultimate stress and strain of in-plane compression elements concerning slenderness and width-to-thickness ratio as well as effective failure length in relation to local buckling effect in a related study [23]. Using ABAQUS software, initial displacement, and residual stress as initial imperfection variables in FE models of beam and shell were examined. The findings showed that local buckling took place in compression members with width-to-thickness ratios greater than 0.7 and that slenderness typically has a greater impact on reducing ultimate stress and strain than does the width-to-thickness ratio. A useful failure length formula was presented to evaluate some of the hugely important regions on the steel compression members. She asserted that the study's findings could be employed to design welded steel compression members for bridges or other structures. Sun et al. [24] reported a numerical and experimental analysis of the local and post-local buckling behavior of welded square high-strength steel tubes with concrete-filled limitations. The experiments indicated that, regardless of the type of steel, the post-buckling reserve strength of tubes employing slender sections rises with the increase of plate slenderness. Based on the results of the finite element (FE) analysis, the slenderness limitations and functional width equations for normal-strength and high-strength steel tubes with concrete-infilled limitations were reported. The comparison found that Song et al. [25] considerably underestimated the slenderness requirement, whereas GB 50936, AS/NZS 2327, and AISC 360–16 overestimated the limitations. The test results were more in line with the specified slenderness limit (0.5), which was rather conservative. The performance of composite tubular steel members has also been extensively studied. Because of the well-known confined and constrained interaction between steel tube and concrete, which results in excellent deformability, these members have been used primarily as bridge piers or columns in high-rise buildings, increasing strength and reducing column size [26, 27].

The criteria for acceptance of different section types based on their section and overall slenderness have not been clearly defined by the standards. The present study involved a sequence of nonlinear finite element analyses aimed at assessing the performance of inelastic tubular column members. This was achieved through the consideration of diverse slenderness and radius-to-thickness ratios, serving as indicators for section slenderness and member slenderness. Then, an attempt to evaluate the acceptance criteria of tubular steel brace in compression of the concentrically braced frame following the general standard provision *ASCE41-17* [28] was tried to develop the presented formulations in this standard. Finally, new formulae were suggested to estimate these acceptance criteria and show their accuracy.

Compressive member actions

Buckling is the most common mode of failure when steel members are subjected to compressive loads [29]. The typical inelastic buckling curve of a compressive brace is presented in Fig. S1 of the supplementary file, which illustrates that the load that induces buckling in inelastic columns is less than the elastic buckling load.

Primary component actions displaying a specific behavior must be categorized as deformation regulated, per *ASCE41-17* standard. The generalized force versus deformation curves utilized in this guideline to provide component modeling and approval standards for deformation-controlled actions can be found in Fig. S2 in the supplementary file. In a relative seismic standard like *ASCE41-17*, the parameters *a*, *b*, and *c* are referred to as variables of acceptance criteria for nonlinear methods.

Brace parameters and review current codes

Mainly tubular sections, while applying as compressive members, are affected by two parameters member slenderness ratio and section slenderness ratio. These parameters influence the buckling and post-buckling behavior of the

column members and, consequently, the ductility evaluation of steel braces. The member's slenderness ratio (λ_c) is provided by:

$$\lambda_c = \sqrt{\frac{\sigma_y}{\sigma_{cr_1}}} = \frac{KL}{r}\frac{1}{\pi}\sqrt{\frac{\sigma_y}{E}} \tag{1}$$

where σ_{cr_1} is flexural buckling stress and can be determined by:

$$\sigma_{cr_1} = \frac{\pi^2 E}{\left(\frac{KL}{r}\right)^2} \tag{2}$$

Furthermore, the normalized section slenderness ratio (λ_c) could be defined for square and circular hollow sections, respectively, as follows:

$$\lambda_s = \sqrt{\frac{\sigma_y}{\sigma_{cr_{2s}}}} = \frac{b}{t}\frac{1}{\pi}\sqrt{3(1-\nu^2)}\frac{\sigma_y}{E} \tag{3}$$

$$\lambda_s = \sqrt{\frac{\sigma_y}{\sigma_{cr_{2c}}}} = \frac{D}{2t}\sqrt{3(1-\nu^2)}\frac{\sigma_y}{E} \tag{4}$$

where,

$$\sigma_{cr_{2s}} = \frac{\pi^2 E}{12(1-\nu^2)}\left(\frac{t}{b}\right)^2 \tag{5}$$

and,

$$\sigma_{cr_{2c}} = \frac{E}{\sqrt{12(1-\nu^2)}}\left(\frac{2t}{D}\right) \tag{6}$$

where ν is the Poisson ratio, E is the Young modulus, σ_y is the yield stress of steel, σ_{cr1} global buckling stress, $\sigma_{cr2,c}$ and $\sigma_{cr2,s}$ are the local buckling stress of circular and square sections, respectively, t is the thickness of cross-section, D is the diameter of circular section, b is the width of the square section, L is member length, and r is gyration radius of the member cross-section.

When the component in compression becomes unstable due to its slenderness and the applied load, the column buckles. According to *ASCE41-17*, performance may be predicted by an inelastic buckling when λ_c is less than 1.5, while behavior above this can be predicted using the Euler formula.

Following *FEMA* [30], the post-buckling strength and acceptance criteria have been defined based on section slenderness. However, it could not be an authentic expression because the post-buckling behavior is an interaction of both section and member slenderness. Then a series of research was carried out [6, 16], and *ASCE41-17* recommended even exact criteria to define the parameters of modeling, brace sections' acceptance criteria, and residual strength ratio. According to *ASCE41-17*, when a member is chubby and section slenderness is less than specific values, for slender member ($KL/r \geq 4.2\sqrt{E/\sigma_y}$ or $\lambda_c \geq 4.2/\pi = 1.33$), the plastic deformation parameters a and b (Fig. 2) are defined as $0.5\Delta_c$ and $9\Delta_c$, respectively. The residual strength ratio (C) of these members is 0.3. (where Δ_c is the axial deformation at the expected buckling load).

For stocky members $KL/r \leq 2.1\sqrt{E/\sigma_y}$ or $\lambda_c \leq 2.1/\pi = 0.67$ the modeling parameters are defined as $a = 1\Delta_c$, $b = 7\Delta_c$ and the residual strength ratio is $c = 0.5$. Moreover, for intermediate slenderness values the acceptance criteria shall be determined by linear interpolation. According to AISC 341–10 (2010), for members with high ductility, the limiting diameter-to-thickness ratio of circular sections shall not exceed $0.038E/\sigma_y$. Also, the limiting width-to-thickness ratio of rectangular sections shall not exceed $0.55\sqrt{E/\sigma_y}$; by substituting these values in Eqs. (3) and (4), respectively, and considering $\nu = 0.3$ for steel materials λ_s is limited as follows for seismically compact sections:

$$\lambda_s \leq \frac{0.038}{2}\sqrt{3(1-\nu^2)} = 0.031\,(\text{For circular Section}) \tag{7}$$

$$\lambda_s \leq \frac{0.55}{\pi}\sqrt{3(1-\nu^2)} = 0.29\,(\text{For circular sections}) \tag{8}$$

Following AISC 360–10 [31], for non-compact members, the limiting diameter-to-thickness ratio of circular sections shall not exceed $0.11E/\sigma_y$. Also, the limiting width-to-thickness ratio of rectangular sections shall not exceed $1.4\sqrt{E/\sigma_y}$; due to similar calculations, λ_s for non-compact sections is:

$$\lambda_s \leq \frac{0.11}{2}\sqrt{3(1-\nu^2)} = 0.09\,(\text{For circular sections}) \tag{9}$$

$$\lambda_s \leq \frac{1.4}{\pi}\sqrt{3(1-\nu^2)} = 0.74\,(\text{For rectangular sections}) \tag{10}$$

According to *ASCE41-17*, the acceptance criterion must be multiplied by 0.5 for non-compact sections.

The acceptance criterion must be multiplied by a number derived from linear interpolation between the seismically compact and non-compact examples for intermediate compactness levels. Consequently, two linear interpolations are required to calculate the acceptance requirements, which is both time-consuming and challenging. This work attempts to suggest new empirical relations to address this flaw.

Cyclic damage and plasticity model

In general, failure in a plastic material is typically outlined in three distinct stages: Accumulation Damage, Damage initiation and Damage Evolution. Following the onset of failure, as evident from area c in Fig. 1, the failure initiates at this point and progresses smoothly towards point *d*, signifying rupture caused by the expansion of damaged microscopic particles.

Abaqus employs various criteria and techniques to anticipate and enhance failure. These include Ductile Damage, Jonson-cook Damage, Shear Damage, FLSD Damage, FLD Damage, M–K Damage, and MSFLD Damage. The choice of method depends on the specific behavior under consideration.

To explore the behavior under cyclic loading and the impact of fatigue resulting from accumulated strain, the most effective approach is MSFLD, also referred to as the Müschenborn-Sonne forming limit diagram method. This method involves defining the ratio of minimum strain to maximum strain, as well as the equivalent strain of a certain path, to identify various types of failure and illustrate them for a specific steel variant. Failure can be predicted by comparing the equivalent strain to the diagram: failure will not occur if the equivalent strain is below the threshold, but if the failure path intersects this region, rupture is anticipated in the specimen (Fig. 2).

According to the ductile damage criterion of the Muschenborn- Sonne Forming Limit Diagram (MSFLD), a cyclic damage plasticity model is developed in this section [32]. Necking, void growth, coalescence, shear fracture owing to shear band localization, and void growth and coalescence are the main processes that can produce ductile metal fracture. The most critical factor in metal forming operations is necking. With the assumption that the forming limit curve reflects the total of the greatest possible equivalent plastic strains, Muschenborn and Sonne provided a technique for forecasting the impact of the deformation path on the forming limits of sheet metals. These presumptions were the foundation for the necking instability of sheet metal criteria utilized in the ABAQUS program [32] for every deformation path. As a result, the Muschenborn-Sonne criteria shifted the original forming limit curve from the space of main against minor strains to the space of comparable plastic strain versus the primary strain ratio (without predeformation influences).

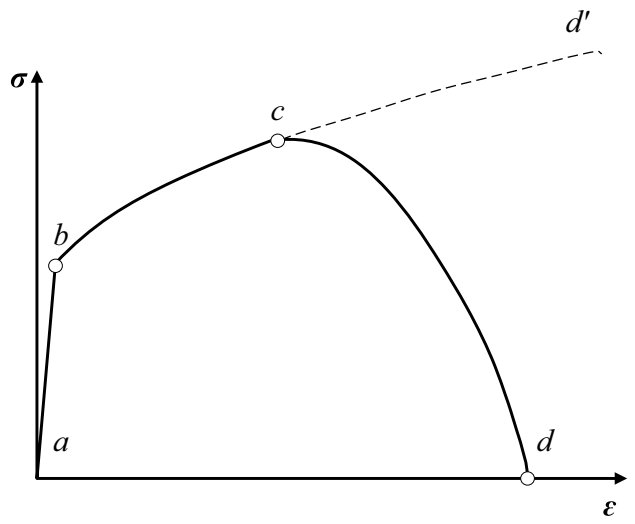

Fig. 1 Soft failure process

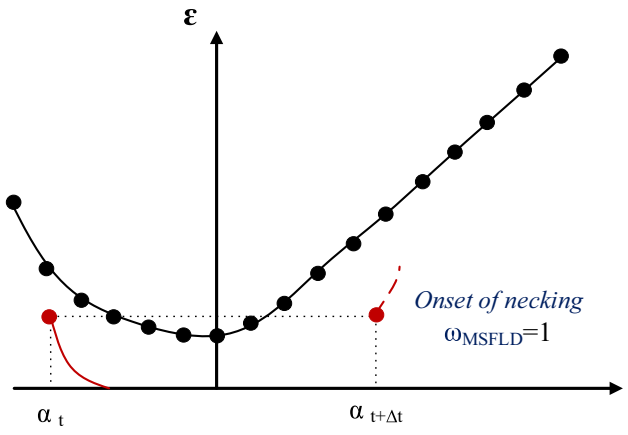

Fig. 2 MSLFD failure criteria curve

Numerical study

Throughout a significant seismic event, steel braces are prone to be damaged through local and global interaction buckling. In order to create a logical seismic design technique and evaluate the ductility of steel braced frames, it is crucial to have a strong knowledge of the inelastic behavior of steel braces. Reliable techniques to forecast the braces' cyclic inelastic large-deflection response are necessary for an accurate cyclic analysis of braced frames [33]. An in-depth study has been done on this, and over the past several decades, several analytical techniques have been created to imitate the hysteretic behavior of braces. The three primary research methods for the cyclic analysis of braces are (1) elastoplastic FE models, (2) plastic-hinge models, and (3) empirical models. FE models that considered geometric and material nonlinearities were used to create more realistic models. The member material and geometry characteristics (constitutive law) are the sole requirements for this procedure, which typically works for many different sorts of issues.

Finite element analysis

A 3D FE model, depicted in Fig. 3, was built using the commercial program ABAQUS to assess the inelastic buckling behavior of steel column members with tubular sections. The models have been developed with reduced integration using four-node shell elements (S4R), with five integration points per element thickness [27]. The S4R mesh type can diminish integration, preventing membrane locking and shearing evenly. The value of maximum imperfection is considered with a factor of 1/1500 of the member length [34–37]. The nonlinear static analysis is performed in ABAQUS as the General Static. The study considers both geometrical and material nonlinearities. As the deformation grows, elements change from their initial forms. The variational concept of virtual work is used to determine the element's stiffness matrix. The study makes use of the displacement control approach in conjunction with the modified Newton–Raphson iteration methodology [38–40]. The formulation and solution technique for large elastoplastic displacements are described in depth in the Reference [41].

Model verification

The numerical FE approach mentioned in the preceding section is used to conduct several numerical studies on steel braces' behavior. The outcomes are contrasted with those of the three standard experiments, *A, B* [41], and *C* [42]. Table 1 provides the specimens' dimensions and shapes. As seen in the table, the characteristics of *A* and *B* specimens are the same, but the load history of all members is different. In order to model boundary conditions and constraints, a reference point is defined at the middle of the end section.

Specimens *A, B*, and *C* were loaded using three different methods. The initial loading history (tests of series A) consisted of a significant compression-tension monocycle with a maximum normalized displacement amplitude ($m = \delta_{max}/\delta_y$), where δ_{max} is the maximum displacement in the compression-half cycle at load reversal and δ_y is the yield displacement corresponding to the squash load of cross section ($\delta_y = \varepsilon_y L = P_y L/EA$, $P_y = A\sigma_y$, A = cross-section area; σ_y = yield stress; L = the length of the brace). Details of the history of applied monocycle loading is presented in Fig. S3 of the supplementary file [43, 44].

The second loading history, which is applied to specimen *B*, is often employed by Japanese academics [45–47] where there is a uniform rise of displacement amplitude (δ_y, $2\delta_y$, $3\delta_y$, etc.) up to failure (δ_y stands for the yield displacement

Table 1 Characteristics of the studied samples

Specimen	Profile	λ_s	λ_c	L (mm)
A	CHS 139.7×3.5(mm)	0.06	0.400	2820
B	CHS 139.7×3.5(mm)	0.06	0.400	2820
C	HSS 6×6x0.375(in)	0.30	0.647	2954

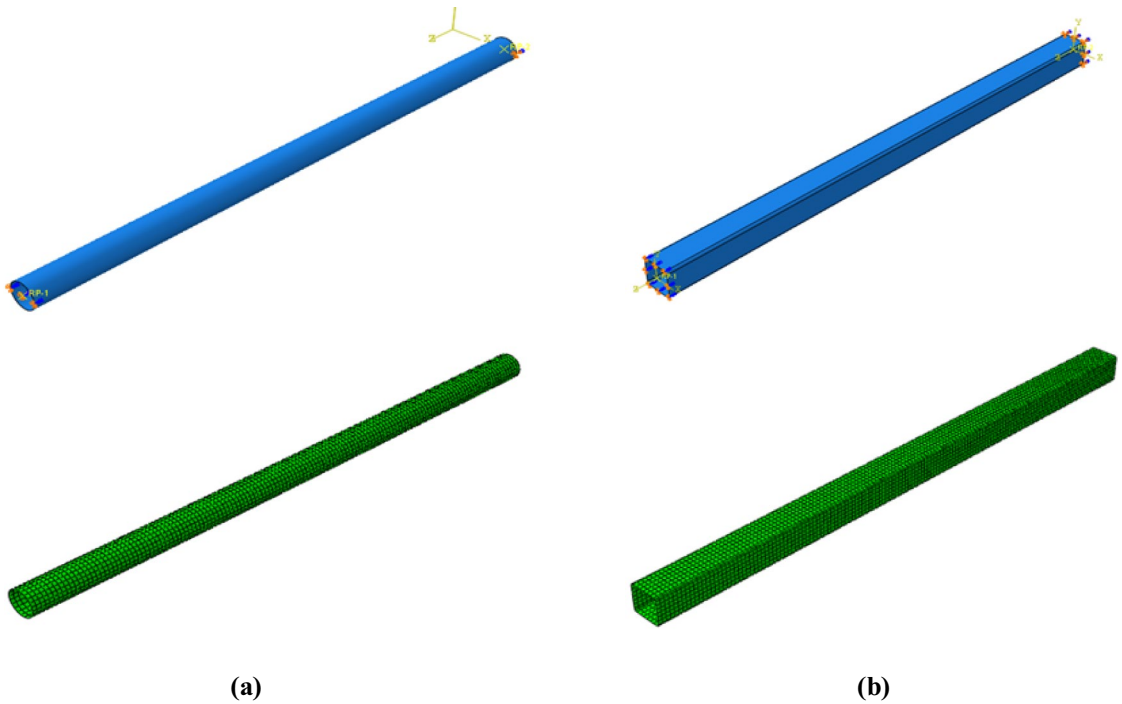

(a) **(b)**

Fig. 3 FE models in ABAQUS, **a** Hollow Circular Steel (HCS) section; **b** Hollow square steel (HSS) section

corresponding to the cross-sectional squash load.). Each amplitude is only repeated once in this scenario (Fig. S4). Elchalakani et al. have prepared the test details [48].

The second loading history was suggested by Huang and Mahin [49]. More information on this loading history is shown in Fig. S5 of the supplementary file. This loading history is applied to specimen *C*.

Cold-formed circular hollow sections made of structural steel with a yield stress of $\sigma_y = 379\ MPa$ and ultimate tensile strength of $\sigma_y = 451\ MPa$ are *AS 1163 grade C350L0* (equal to *ASTM A500* tubes). Steel's material nonlinearity is taken into account during material modeling by providing an accurate stress–strain curve with the correct input format for ABAQUS in terms of real stress and plastic strain. The material's strain-hardening behavior in the plastic range is the critical behavior of structural steel to be considered [50]. As a result, a model that coupled kinematic and isotropic strain hardening was adopted. The material has Young's modulus and Poisson's ratio of 200,000 MPa and 0.3, respectively. The investigation used a tri-linear stress–strain material model. The strain hardening modulus is considered 2% of the initial Young modulus and with a maximum elongation of 2% (more details in Fig. S6 in the supplementary file). The typical material property *ASTM A500 Grade B* steel is utilized for the specimen *C*. The detail of the material property is described by Yang and Mahin [42].

In order to validate the results, specimen A is modeled by the ABAQUS software, and the results are compared with those in tests [41]; Fig. 4 shows a slight discrepancy between experimental and analytical strength degradation under tension load. The brace behaves as expected up until a substantial decline in estimated tensile strength occurs beyond this displacement. This sharp drop in predicted tensile strength may be caused by creating a plastic hinge at the member's mid-span under combined biaxial hoop stress and axial stress.

Numerical analyses have been done for typical B series, and the result is verified for the test (Fig. 3). The experimental data is extracted from the test by Elchlakani [48]. Furthermore, numerical analyses have been done for the *C* series test, and the result compares with the test Yang and Mahin reported [42] (see Fig. 5).

Specimens have been analyzed, such data is obtained, and target displacement and referred strength ratio are derived. Then, the relationship between the buckling strength of the brace member and the slenderness parameter. The residual strength ratio and target displacement relationship are calculated from the load-deformation curve and slenderness parameters. These findings suggest that the numerical analysis's FE modeling may reasonably anticipate the cyclic behavior of axially loaded fixed-end steel braces with circular hollow sections that have been seen experimentally. The stresses and deformed arrangement of the HSS and HCS sections in ABAQUS are shown in Figs. 6 and 7. As can be observed, under compression force, local buckling at the center is followed by global buckling. At the brace's

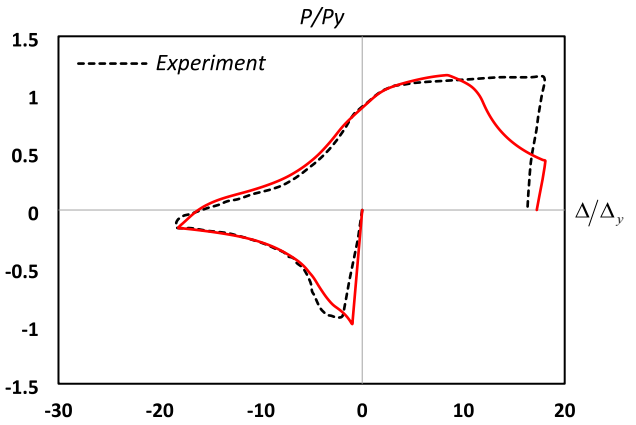

Fig. 4 Comparison between experiment and FE simulation for specimen A

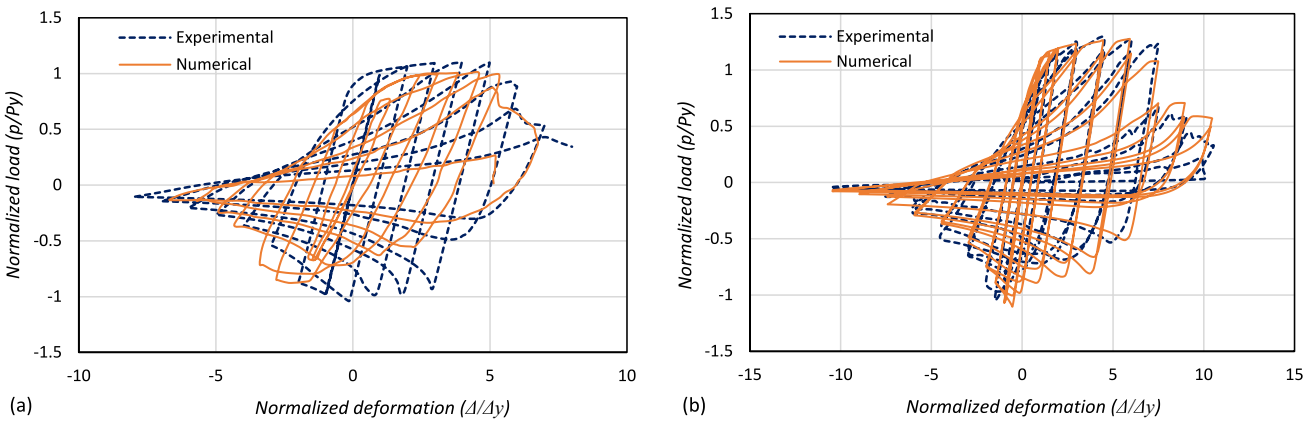

Fig. 5 Comparison between FE simulation and experiment for specimen (**a**) B and **b** C

midspan, a tear-through failure mode occurs during compression force.

Proposed relations for seismic behavior of braces

As stated in previous sections, the inelastic performance of a brace member (target displacements (a, b) and residual strength ratio (c)) depends on two parameters: section slenderness and member slenderness. In order to obtain empirical relations, it is necessary to have the results of bracing members' behavior in a wide range of thicknesses and dimensions. To do this, ABAQUS software has carried out a series of numerical simulations of members with a range of $18 \leq KL/r \leq 180$ ($0.25 \leq \lambda_c \leq 2.5$) and different section slenderness (2013). The total number of specimens is 594, as follows (Table 2);

For HCS:7 *diameters* $(d) \times 6$ *thicknesses* $(t) \times 9$ *slenderness ratios* $(Kl/r) = 378$;

For HSS:4 *depths* $(b) \times 6$ *thicknesses* $(t) \times 9$ *slenderness ratios* $(Kl/r) = 216$.

Figure 8 shows the normalized axial strength of circular specimens against the normalized target displacement for various slenderness ratios with seismically compact sections.

As seen in the figure, when the member slenderness varies from 38.5 to 98.5, the post-buckling strength is lower than in other specimens. In this range, first, the global buckling accrues, and then local buckling and yielding occur and cause a sharp reduction and sudden drop in strength. For slenderness less than 38.5, the member does not have a global buckling. In this case, yielding accrues first, and then local buckling happens. When local buckling starts, the section acts like a plate due to being short and can tolerate more load after buckling. The post-buckling behavior of such members with low slenderness is outstanding so that they buckle softly; moreover, the sharp drop in post-buckling strength of those is lower. For slendernesses more than 98.5, the members have little bearing capacity. Even though the compressive stresses of those are low, they have geometric

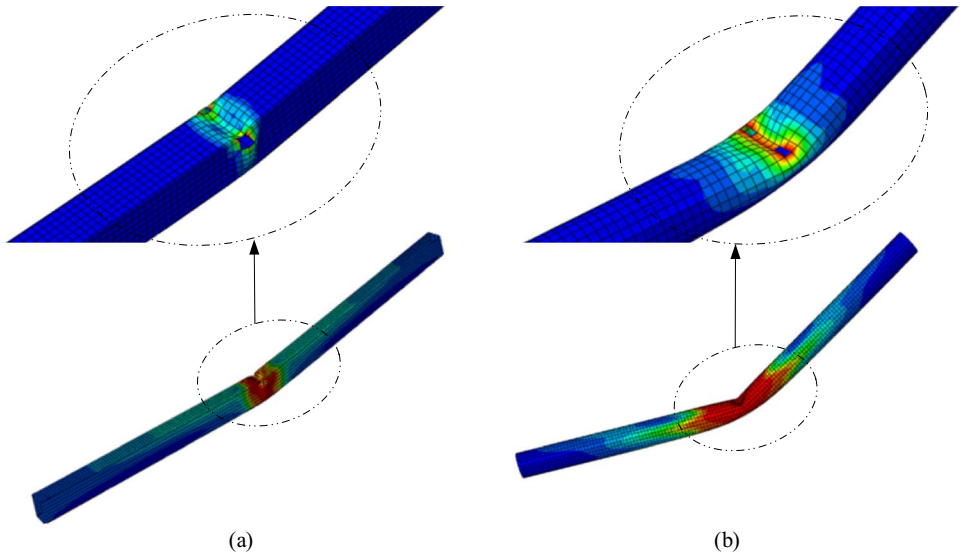

(a) (b)

Fig. 6 Deformed configuration in ABAQUS: **a** HSS section, and **b** HCS section

(a) (b)

Fig. 7 Experimental deformed configuration: **a** HSS section, and **b** HCS section

Table 2 Specifications and details of specimens

Specimen	D or b (mm)	t (mm)	kl/r	Total analyses
HCS d×t			18.50	7×6×9=378
	60.30	3.50	38.50	
	101.60	4.00	58.50	
	139.70	4. 50	78.50	
	219.10	6.04	98.50	
	273.10	7.52	118.50	
	323.90	12.00	138.50	
	406.40		158.50	
			178.50	
HSS b×t			18.50	4×6×9=216
	100.00	3.50	38.50	
	150.00	4.00	58.50	
	200.00	4. 50	78.50	
	250.00	6.04	98.50	
		7.52	118.50	
		12.00	138.50	
			158.50	
			178.50	

nonlinear behavior. The local buckling of such members occurs late; besides, they have good post-bulking behavior.

For slendernesses, less than 38.5, which have inconsistent behavior in post-buckling, as shown in Fig. 8, a separate Figure (Fig. 9) depicts various slenderness in order to illustrate their response meticulously. As shown in the figure, post-buckling strength increases when member slenderness decreases; due to reducing the buckling length, the behavior of these members is similar to cylindrical shells. Figure 10 shows the normalized axial strength of the box specimen against the normalized target displacement. As shown in the figure, with increasing slenderness from 18 to 88, the post-buckling strength is reduced, whereas the post-buckling strength increases for slenderness more than 88.

Furthermore, in Fig. 11, the values of parameter a are shown for circular sections in different slenderness.

In an attempt detailed herein, logical equations have been sought through the assessment of bracing elements' post-buckling behavior and residual strength ratio. The graphical representation in Fig. 12 illustrates the relationship between the residual strength ratio (c) and the slenderness of the elements. It is evident that, in general, lower values of λ_c correspond to higher values of the residual strength ratio (c). As the parameter λ_c increases, the residual strength ratio diminishes until λ_c reaches 1.33; subsequently, the ratio begins to rise with the escalation of member slenderness. It is important to highlight that the AB and EF lines delineate sections categorized as seismically compact and non-compact for robust members, respectively, whereas the CD line pertains to slender elements. Moreover, the FC and BC lines serve to distinguish seismically compact and non-compact sections, bridging the slender segment to the robust members.

However, it is not a fact that when λ_c is less than 1.33, inelastic behavior is affected by section slenderness. The target displacement could be varied due to any changes in λ_s. Therefore, residual strength ratio (c) shall be defined in terms of target displacement employing 3-D coordinates. In Fig. 13, the b-axis indicates normalized target

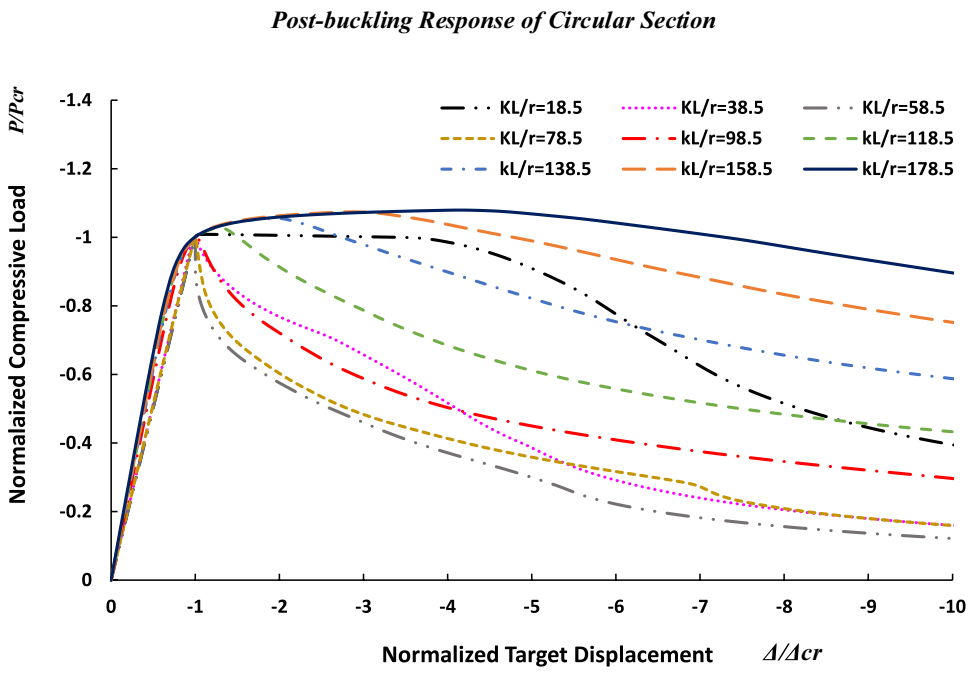

Fig. 8 Post-buckling response of circular sections in different slenderness ratios with seismically compact section

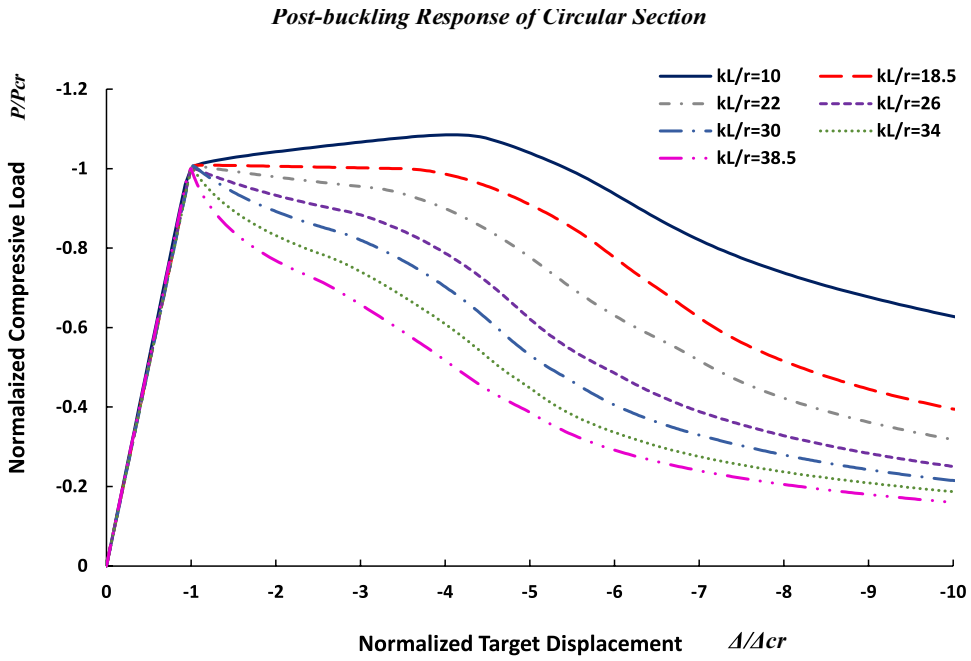

Fig. 9 Post-buckling response of circular sections in different slenderness ratios with seismically compact section

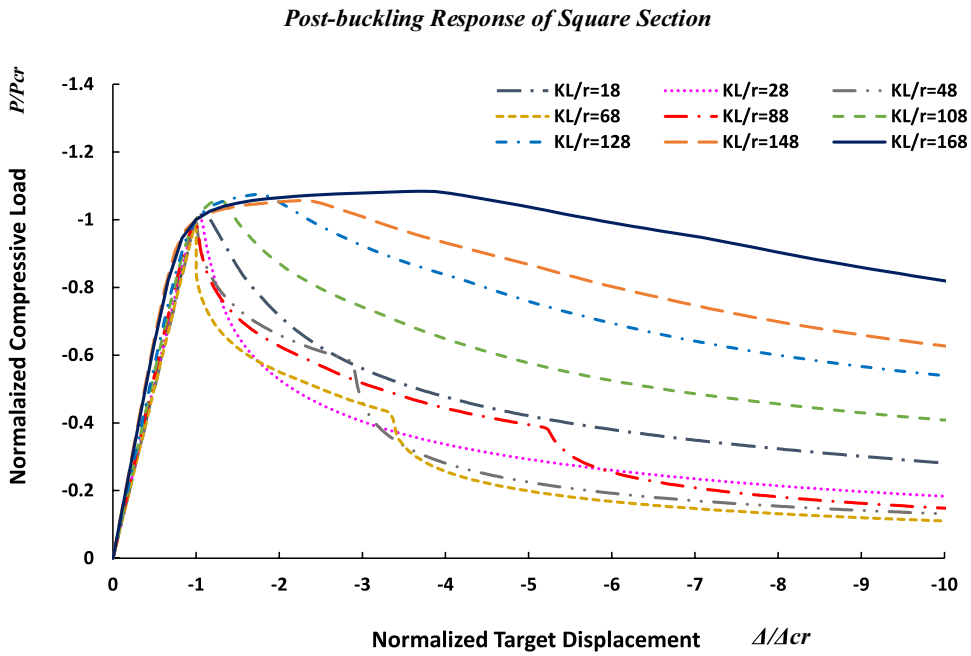

Fig. 10 Post-buckling response of square sections in different slenderness ratios with seismically compact section

displacement (Δ/Δ_{cr}), where Δ_{cr} is the axial deformation at the expected buckling load.

The *AB* and *EF* lines refer to seismically compact and non-compact sections, which for stocky members could be defined by Eqs. (11) and (12), respectively.

$$\begin{cases} c = 1.391862 - 1.04155\lambda_c - 3.0496\lambda_c^2 + 3.6705\lambda_c^3 \\ b = 8 \end{cases} \tag{11}$$

$$\begin{cases} c = 1.8346 - 5.453\lambda_c + 6.2749\lambda_c^2 - 2.3554\lambda_c^3 \\ b = 4 \end{cases} \tag{12}$$

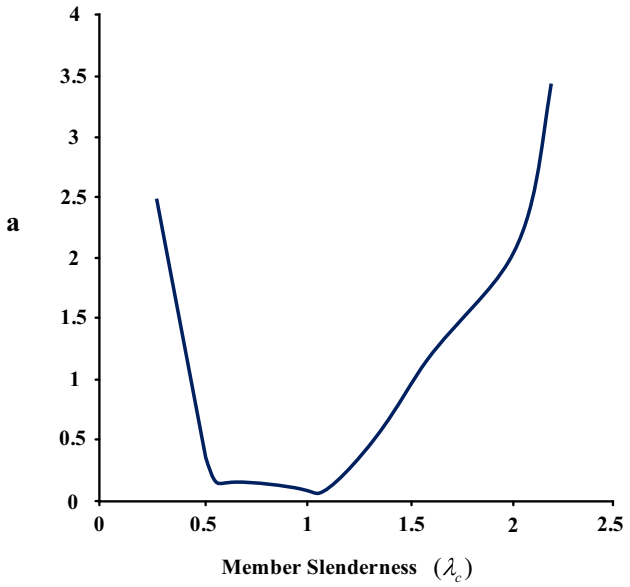

Fig. 11 The values of parameter a for circular sections in different slenderness ratios

The *CD* line in Fig. 13 refers to slender members. It could be comprehensive that the section slenderness ratio has no impact on the residual strength ratio, so the following Equation derives it.

$$\begin{cases} c = 2.8147 - 5.9107\lambda_c + 5.64036\lambda_c^2 - 9.0052\lambda_c^3 \\ b = 8 \end{cases} \quad (13)$$

For members that are seismically compact and non-compact $0.67 \le \lambda_c \le 1.33$, the residual strength ratio could be estimated by 3D line equations that connect the slender part to stocky members. Equations (14) and (15) refer to *FC* and *BC* lines utilized for seismically compact and non-compact sections, respectively.

$$\begin{cases} c = -0.23\lambda_c + 0.57 \\ b = 9.1\lambda_c - 2.1 \end{cases} \quad (14)$$

$$\begin{cases} c = -0.015\lambda_c + 0.31 \\ b = 3.03\lambda_c + 5.97 \end{cases} \quad (15)$$

Between seismically compact and non-compact sections, a surface could be estimated. For more understanding of this, a 3D surface is plotted in Fig. 14.

Based on Figs. 12, 13 and 14 it can inferred that there exists an intricate correlation between the cross-sectional slenderness and the post-buckling resistance of member slenderness, as well as the target displacement. This issue is not explicitly addressed in standards such as ASCE and FEMA, which only recommend the use of linear interpolation for determination purposes. In cases where the member exhibits slenderness (i.e., when kl / r is high), the compression of the cross-section does not impact the post-buckling resistance. The applied deformation (b) in such scenarios closely resembles that of a slender member, whether the cross-section is compacted or not, resulting in equal post-buckling strength. Conversely, for a stocky member (where $\lambda c \le 0.67$), the influence of cross-sectional slenderness is substantial. The alteration of a compact cross-section significantly affects the target displacement. The impact is more

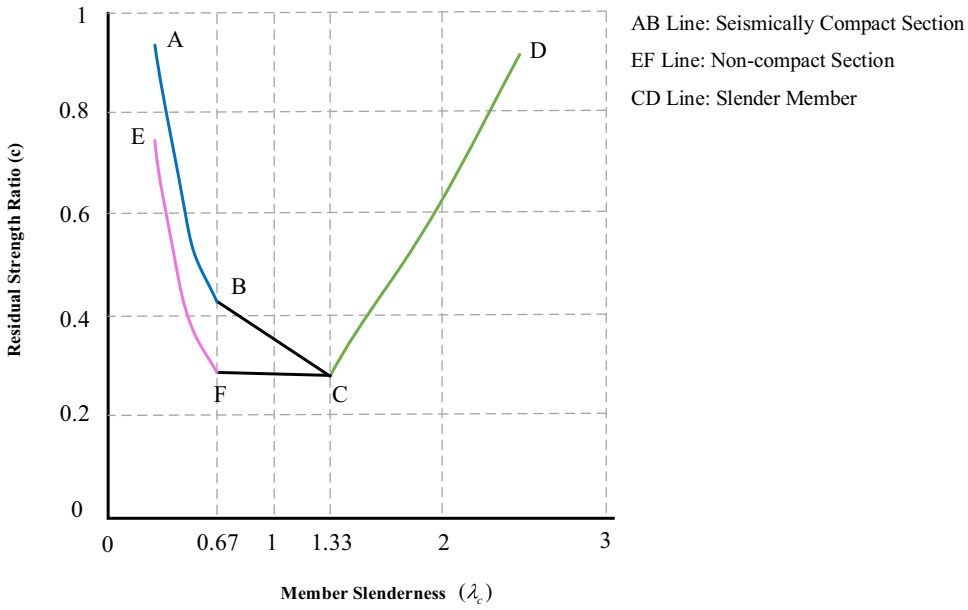

Fig. 12 Tow-dimensional relationship post-buckling acceptance criteria and slenderness

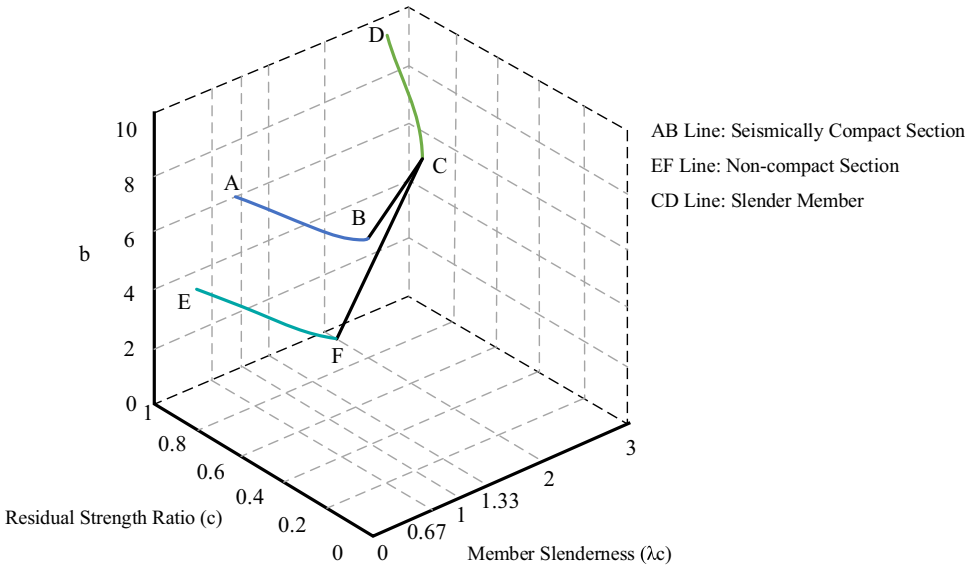

Fig. 13 Three-dimensional relationship post-buckling acceptance criteria and slenderness

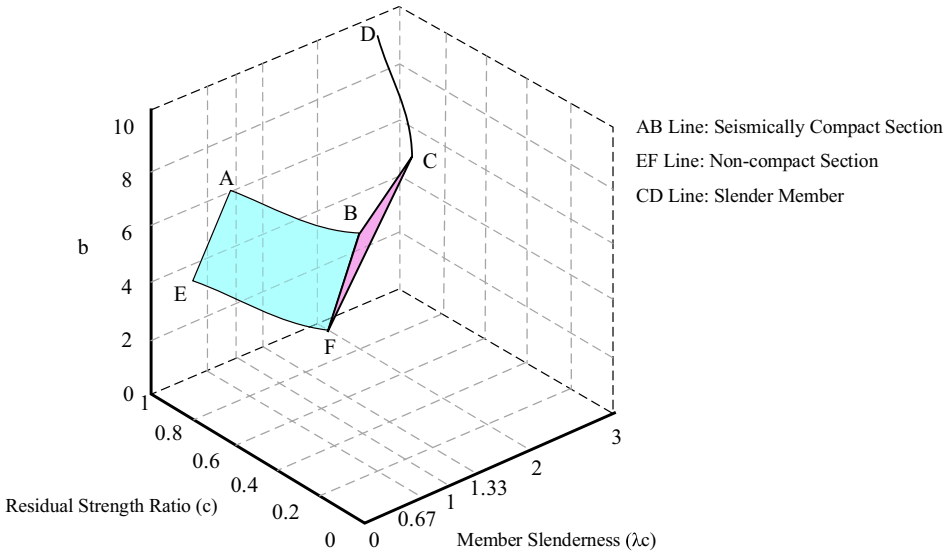

Fig. 14 The 3D surface between seismically compact and non-compact sections

pronounced in comparison to a non-compacted member when aiming to attain the target post-buckling resistance (as shown on the axis of the three-dimensional figure). A non-compacted section, due to local buckling, swiftly transitions from a stable state to achieving post-buckling strength. In the transitional region between stocky and slender members, the effects of cross-sectional compression gradually diminish, eventually reaching a point where cross-sectional compression is negligible. At this stage, the applied deformation has no effect, and the post-buckling strength remains constant.

Summary, conclusion, and limitations

In order to evaluate the inelastic behavior of hollow steel brace sections, a sequence of *FE* calculations was conducted using the member and section slenderness as factors. The findings of the cyclic loading test were used to verify the analysis model. According to the comparison outcome, the load-deformation relationship and the inelastic buckling mode were in strong agreement. Additionally, the impact of the slenderness ratio on inelastic buckling behavior was examined. Observations show that, for members with slenderness, $\lambda_c \leq 0.67$, local buckling has a significant effect on ductility and final collapse. For slender members $\lambda_c \geq 1.33$, local buckling almost does not affect post-buckling strength.

When the value λ_c is low, the residual strength ratio (c) is high. With increasing λ_c, the residual strength ratio reduces until $\lambda_c = 1.33$, and then with the rise of member slenderness, the residual strength ratio increases.

For stocky members ($\lambda_c \leq 0.67$) with sections seismically compact and non-compact and slender members ($\lambda_c \geq 1.33$), some rational relations are proposed to simulate the residual strength ratio and target displacement. For seismically compact and non-compact members with $0.67 \leq \lambda_c \leq 1.33$, the residual strength ratio could be estimated by 3D line equations connecting the slender part to the stocky part. Separate equations, which are utilized for seismically compact and non-compact sections, are provided.

It has been inferred that the finite element modeling and numerical approach employed in numerical analysis are capable of estimating with a similar level of accuracy as experimental measurements. In subsequent investigations, the given equations should be verified or confirmed using experimental or numerical data. For the purpose of future research endeavors, it is advised to utilize experimental examinations in order to enhance and validate the numerical findings pertaining to the impact of section slenderness and member slenderness on the inelastic response of tabular sections in bracing elements.

It is crucial to recognize that due to its emphasis on a simplified issue, the study is fundamentally oriented, with its primary significance lying in illustrating the influence of section slenderness and member slenderness on the inelastic behavior of tabular sections within bracing components. Consequently, the formulation per se is not readily extensible to structural issues except for those bearing a close resemblance to the cases analyzed here in relation to their geometric or material characteristics.

Supplementary Information The online version contains supplementary material available at https://doi.org/10.1007/s41062-024-01667-3.

Funding The authors declare that no funds, grants, or other support were received during the preparation of this manuscript.

Declarations

Conflict of interest The authors have no relevant financial or non-financial interests to disclose.

References

1. Farhangi V, Jahangir H, Eidgahee DR et al (2021) Behaviour investigation of SMA-equipped bar hysteretic dampers using machine learning techniques. Appl Sci 11:10057
2. Mohammed AH, Mubarak HM, Hussein AK et al (2022) Punching shear characterization of steel fiber-reinforced concrete flat slabs. HighTech Innov J 3:483–490. https://doi.org/10.28991/HIJ-2022-03-04-08
3. Park HM, Choi JH (2011) Evaluation on the post-buckling residual strength of H-shaped steel column. Proc Eng 10:3387–3392. https://doi.org/10.1016/j.proeng.2011.04.558
4. Shahraki M, Darmiyan HM (2023) Structural behaviors of strengthened deficient steel square hollow section columns under axial compressive loads. Innov Infrastruct Solut 8:1. https://doi.org/10.1007/s41062-022-00955-0
5. Makhdoumi Darmian H, Rahgozar R, Mohammadizadeh M et al (2022) Post-fire evaluation of SHS retrofitted steel columns. Innov Infrastruct Solut 7:133. https://doi.org/10.1007/s41062-021-00732-5
6. Yu C, Schafer BW (2002) Local buckling tests on cold-formed steel beams. Int Spec Conf Cold-Formed Steel Struct Recent Res Dev Cold-Formed Steel Des Constr 129:127–144. https://doi.org/10.1061/(asce)0733-9445(2003)129:12(1596)
7. Gjukaj A, Salihu F, Muriqi A, Cvetanovski P (2023) Numerical behavior of extended end-plate bolted connection under monotonic loading. HighTech Innov J 4:294–308. https://doi.org/10.28991/HIJ-2023-04-02-04
8. Mahmoudi M, Zaree M (2011) Evaluating the overstrength of concentrically braced steel frame systems considering members post-buckling strength. Int J Civ Eng 9:57–62
9. Bruneau M, Uang C-M, Sabelli R (2005) Ductile design of CBF steel structures. Improvement of buildings' structural quality by new technologies, 2nd edn. CRC Press, New York, pp 641–650
10. Galambos TV (1998) Guide to stability design criteria for metal structures. John Wiley & Sons, Hoboken
11. Tang X, Goel SC (1989) Brace fractures and analysis of phase I structure. J Struct Eng 115:1960–1976. https://doi.org/10.1061/(asce)0733-9445(1989)115:8(1960)
12. Hassan OF (1991) Modeling of bracing members and seismic behavior of concentrically braced steel structures. University of Michigan PP, United States
13. Tremblay R (2000) Influence of brace slenderness on the seismic response of concentrically braced steel frames. Behaviour of steel structures in seismic areas. CRC Press, London, pp 527–534
14. Jain, Ashok K. and SCG (1978) Hysteresis models for steel members subjected to cyclic buckling or cyclic end moments and buckling (User's guide for DRAIN-2D: EL9 and EL10)
15. Lee S, Goel SC (1987) Seismic behaviour of hollow and concretefilled square tubular bracing members, UMCE 87–11. Michigan, Ann Arbor
16. Tremblay R (2002) Inelastic seismic response of steel bracing members. J Constr Steel Res 58:665–701. https://doi.org/10.1016/S0143-974X(01)00104-3
17. Fell BV (2008) Large-scale testing and simulation of earthquake-induced ultra low cycle fatigue in bracing members subjected to cyclic inelastic buckling
18. Chen C, Mahin SA (2012) Pacific earthquake engineering performance-based seismic demand assessment of concentrically braced steel frame buildings
19. Haddad RTM, Martinez G, Richard J, Moffatt K (2008) Inelastic cyclic testing of large size steel bracing members. 14 World Conf Earthq Eng
20. Kumar PCA, Sahoo DR, Kumar N (2015) Limiting values of slenderness ratio for circular braces of concentrically braced frames. J Constr Steel Res 115:223–235. https://doi.org/10.1016/j.jcsr.2015.08.026
21. Dey P, Gupta RK, Laskar AI (2019) Numerical and experimental investigations of different cross-sectional configuration of plain concrete and CFST short columns under axial compression. Int J Civ Eng 17:1585–1601. https://doi.org/10.1007/s40999-019-00427-0
22. Song H, Liu J, Yang Y, Chen YF (2019) Study on mechanical behavior of integrated multi-cell concrete-filled steel tubular

stub columns under concentric compression. Int J Civ Eng 17:361–376. https://doi.org/10.1007/s40999-018-0367-z
23. Susanti L (2022) Ultimate strength and ductility of welded box-section compression members. Asian J Civ Eng 23:87–98. https://doi.org/10.1007/s42107-021-00410-y
24. Sun L, Liu Y, Wang H, Shi F (2023) Local and post-local buckling behavior of welded square high-strength steel tubes with concrete-infilled restraints. Thin-Walled Struct 183:110381. https://doi.org/10.1016/j.tws.2022.110381
25. Song Y, Li J, Chen Y (2019) Local and post-local buckling of normal/high strength steel sections with concrete infill. Thin-Walled Struct 138:155–169. https://doi.org/10.1016/j.tws.2019.02.004
26. Rajić A, Lukačević I, Skejić D, Ungureanu V (2023) Cold-formed steel-concrete composite beams with back-to-back channel sections in bending. Civ Eng J 9:2345–2369
27. Güllü A, Danquah JO, Dilibal S (2022) Characterization of energy dissipative cushions made of Ni-Ti shape memory alloy. Smart Mater Struct 31:015018. https://doi.org/10.1088/1361-665X/ac383d
28. ASCE standard, ASCE/SEI 41–17 (2017) Seismic evaluation and retrofit of existing buildings
29. Soleymani A, Saffari H (2023) Seismic improvement and rehabilitation of steel concentric braced frames: a framework-based review. J Rehabil Civ Eng 11:153–177. https://doi.org/10.22075/JRCE.2022.26179.1611
30. Prestandard F (2000) commentary for the seismic rehabilitation of buildings (FEMA356). DC Fed Emerg Manag Agency, Washington, p 7
31. AISC Committee (2010) Specification for Structural Steel Buildings, Standard No. ANSI/AISC 360–10
32. SIMULIA A (2013) analysis and theory manuals. Providence (RI, USA): SIMULIA, the Dassault Systèmes, Realistic Simulation
33. Chen J, Zhang DW, Jin WL (2015) Concrete-filled steel and steel tubular T-joints under cyclic in-plane bending. Adv Struct Eng 18:2207–2216. https://doi.org/10.1260/1369-4332.18.12.2207
34. Usami T, Itoh Y (1998) Stability and ductility of steel structures. Elsevier, Amsterdam
35. Elani M, Temsah Y, Ghanem H et al (2018) The effect of shear reinforcement ratio on prestressed concrete beams subjected to impact load. Proc Int Struct Eng Constr. https://doi.org/10.14455/ISEC.res.2018.55
36. Temsah Y, Jahami A, Aouad C (2021) Silos structural response to blast loading. Eng Struct 243:112671. https://doi.org/10.1016/j.engstruct.2021.112671
37. Temsah Y, Jahami A, Khatib J, Sonebi M (2018) Numerical analysis of a reinforced concrete beam under blast loading. MATEC Web Conf 149:02063. https://doi.org/10.1051/matecconf/201714902063
38. Zienkiewicz OC (1977) The finite element method: 3d Expanded and Rev. ed. McGraw-Hill
39. Al Rawi Y, Temsah Y, Ghanem H et al (2018) The effect of impact loads on prestressed concrete slabs. Proc Int Struct Eng Constr. https://doi.org/10.14455/ISEC.res.2018.54
40. Jahami A, Halawi J, Temsah Y, Jaber L (2023) Assessment of soil-structure interaction effects on the beirut port silos due to the 4 August 2020 explosion: a coupled Eulerian–Lagrangian approach. Infrastructures 8:147. https://doi.org/10.3390/infrastructures8100147
41. Mamaghani IHP, Usami T, Mizuno E (1996) Cyclic elastoplastic large displacement behavior of steel compression members. J Struct Eng A 42:135–145
42. Yang F, Mahin SA (2005) Limiting net section failure in slotted HSS braces. Struct Steel Educ Counc Moraga, CA 20:2005
43. Krawinkler H, Parisi F, Ibarra L, et al (2000) Development of a testing protocol for wood frame structures, CUREE Publication No. W-02, Calif
44. Krawinkler H, Gupta A, Medina R, Luco N (2000) Development of loading histories for testing of steel beam to column assemblies. Stanford University
45. Zheng Y, Usami T, Ge H (2000) Ductility evaluation procedure for thin-walled steel structures. J Struct Eng 126:1312–1319. https://doi.org/10.1061/(asce)0733-9445(2000)126:11(1312)
46. Usami T, Ge HB (1998) Cyclic behavior of thin-walled steel structures - Numerical analysis. Thin-Walled Struct 32:41–80. https://doi.org/10.1016/s0263-8231(98)00027-5
47. Usami T, Banno S, Zetsu H, Aoki T (1993) An experimental study on elasto-plastic behaviour of compression members under cyclic loading—effect of loading program. J Struct Eng A JSCE 39:235–247
48. Elchalakani M, Zhao X-L, Grzebieta R (2003) Tests of cold-formed circular tubular braces under cyclic axial loading. J Struct Eng 129:507–514. https://doi.org/10.1061/(asce)0733-9445(2003)129:4(507)
49. Huang Y, Mahin SA (2010) PEER 2010/104Simulating the inelastic seismic behavior of steel braced frames including the effects of low-cycle fatigue. University of California, Berkeley
50. Chan C, Yu T, Zhang S (2018) Compressive behaviour of square fibre-reinforced polymer–concrete–steel hybrid multi-tube concrete columns. Adv Struct Eng 21:1162–1172. https://doi.org/10.1177/1369433217732499